Equation of State of CO_2 Shock Compressed to 1 TPa

L. E. Crandall,[1,2] J. R. Rygg,[1,2,3] D. K. Spaulding,[4] T. R. Boehly,[1] S. Brygoo,[5] P. M. Celliers,[6] J. H. Eggert,[6] D. E. Fratanduono,[6] B. J. Henderson,[1,2] M. F. Huff,[1,2] R. Jeanloz,[7] A. Lazicki,[6] M. C. Marshall,[6] D. N. Polsin,[1] M. Zaghoo,[1] M. Millot,[6] and G. W. Collins[1,2,3]

[1]*Laboratory for Laser Energetics, Rochester, New York 14623, USA*
[2]*Department of Physics, University of Rochester, Rochester, New York 14611, USA*
[3]*Department of Mechanical Engineering, University of Rochester, Rochester, New York 14611, USA*
[4]*University of California, Davis, California 95616, USA*
[5]*CEA, DAM, DIF, F-91297 Arpajon, France*
[6]*Lawrence Livermore National Laboratory, Livermore, California 94550-9234, USA*
[7]*University of California, Berkeley, California 94720-5800, USA*

(Received 5 May 2020; accepted 31 August 2020; published 14 October 2020)

Equation-of-state (pressure, density, temperature, internal energy) and reflectivity measurements on shock-compressed CO_2 at and above the insulating-to-conducting transition reveal new insight into the chemistry of simple molecular systems in the warm-dense-matter regime. CO_2 samples were precompressed in diamond-anvil cells to tune the initial densities from 1.35 g/cm^3 (liquid) to 1.74 g/cm^3 (solid) at room temperature and were then shock compressed up to 1 TPa and 93 000 K. Variation in initial density was leveraged to infer thermodynamic derivatives including specific heat and Gruneisen coefficient, exposing a complex bonded and moderately ionized state at the most extreme conditions studied.

DOI: 10.1103/PhysRevLett.125.165701

At terapascal pressures (10 million atm), forces on atoms and molecules are comparable to their intrinsic quantum forces. Carbon dioxide is a simple molecular species with strong and stable chemical bonds at ambient conditions that exhibits complex phase transition behavior under increasing pressure and temperature. The physical, chemical, and thermodynamic behaviors of simple molecules comprising H, C, O, and N at hundreds of GPa and thousands of kelvin are vital to unraveling the dynamo, convective flow, and evolution of giant planets [1–3]. Additionally, CO_2 is an important by-product of reacted chemical explosives and its polarity, conductivity, and diffusivity at high pressure dictate the reactive dynamics of these explosives [4,5]. The phase diagram of solid carbon dioxide has been extensively studied with heated diamond-anvil cells (DACs) to 120 GPa [6–11]. The present work demonstrates that the warm-dense-fluid regime of CO_2 is equally complex up to TPa pressures.

Previous shock wave data on initially liquid CO_2 ($\rho_0 = 1.17$ g/cm^3) up to 71 GPa [12,13] reveal a deflection in the Hugoniot (locus of material states attainable with a single shock wave) above 30 GPa, which is thought to indicate the onset of molecular dissociation or polymerization. Shock wave data on initially solid CO_2 ($\rho_0 = 1.45$ g/cm^3) [14,15] extend to 63 GPa and do not exhibit molecular bonding changes. More recently, dynamic compression experiments at the Sandia Z Facility measured the Hugoniot of liquid CO_2 ($\rho_0 = 1.17$ g/cm^3) to 840 GPa [16], which was found to compare well with *ab initio* calculations. These experiments measured the mechanical response of CO_2, and relied on theory to infer thermodynamic behavior. We present the first temperature and reflectivity measurements of shocked CO_2.

This work uses precompression and laser-driven shocks to explore the CO_2 equation of state (EOS) over a wide range of pressures and temperatures, extending to 1 TPa (10 Mbar) and 93 000 K (8 eV). CO_2 was precompressed to pressures up to 1.16 GPa in DACs, attaining both liquid and solid initial states, and was then shock compressed. The temperature-pressure-density-internal energy (T, P, ρ, E) EOS and optical reflectance (R) at 532 nm for these shocks were obtained with a velocity interferometer and an optical pyrometer. These data map a broad range of states from which thermodynamic derivatives were inferred, including the specific heat (c_v) and the Gruneisen coefficient (γ).

Combining these new data with previous results and theoretical calculations [17] reveals a rich and complex phase diagram for CO_2. The shocked fluid exhibits at least three linear slopes in the shock velocity versus particle velocity plane; this may indicate three distinct phases, or two phases with a transition region. Optical reflectivity measurements reveal an insulator-to-conductor transition between 100 and 200 GPa with a carrier density of roughly 0.3 e^-/atom. The observed trend in specific heat suggests a complex bonded fluid with increasing molecular degrees of freedom up to 1 TPa, as opposed to an atomic fluid.

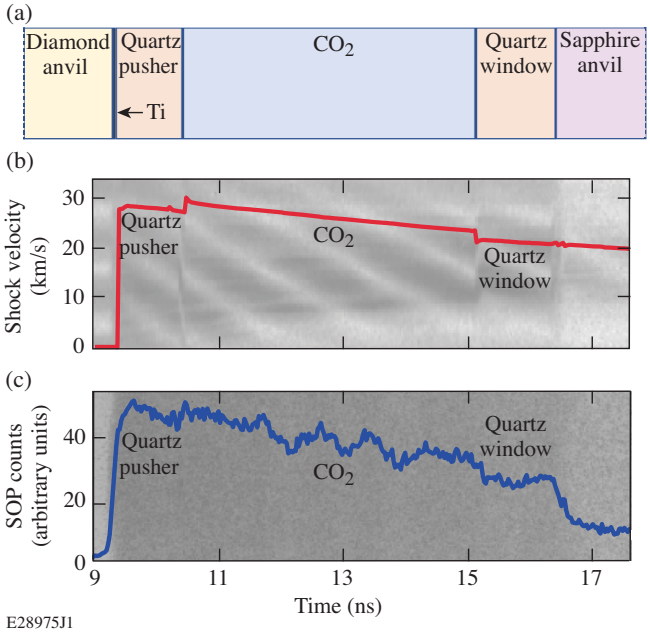

FIG. 1. (a) A schematic of the target: CO_2, sandwiched between quartz references, is precompressed in diamond-sapphire anvil cells to a liquid or solid-I phase before being dynamically compressed with laser-driven shock waves. (b),(c) Raw VISAR/SOP streaked images from shot 58 922. Overplotted are shock velocity (red) and raw SOP count (blue) temporal profiles. VISAR: velocity interferometer system for any reflector; SOP: streaked optical pyrometer.

We find that state-of-the-art modeling needs refinement to match the observed reflectivity and compressibility behavior of CO_2. High-pressure chemistry was once believed to be rather simple, and characterized by ions embedded in a sea of electrons. The present work, however, reveals that chemical bonding—inhomogeneities in the electron fluid—can still be significant at TPa conditions.

These shocked CO_2 experiments were performed at the OMEGA Laser Facility at the Laboratory for Laser Energetics at the University of Rochester [18]. CO_2 samples were precompressed to various initial pressures [19] using DACs [20–23] to explore a family of Hugoniots. A schematic of the cell is shown in Fig. 1(a). CO_2 was cryogenically loaded into cells comprising diamond and sapphire anvils before being mechanically precompressed to initial densities (ρ_0) ranging from 1.35 g/cm^3 (liquid [24]) to 1.74 g/cm^3 (solid-I [10]). A gold x-ray shield and a CH plastic ablator (not shown in the schematic) were deposited onto the diamond. Two α-quartz references were inserted on either side of the CO_2 sample. The OMEGA laser irradiated the diamond side of the DAC with intensities up to 8×10^{14} W/cm^2 to drive shock waves with up to TPa pressures into the precompressed CO_2.

The velocity of the reflecting shock wave was measured throughout the shock transit of the entire experiment with a dual-channel velocity interferometer system for any reflector (VISAR) [25]. The quartz pusher was used as a reference [26–28] for impedance matching [29] at the pusher-CO_2 interface to determine the pressure and particle velocity of shocked CO_2. In one shot, a fused-silica pusher served as the reference [30–33]. Density and internal energy were then determined from the Rankine-Hugoniot conservation relations. Uncertainty in the particle velocity, pressure, density, and internal energy were propagated from random experimental uncertainties and systematic uncertainties from the quartz reference with a 100 000 trial Monte Carlo method [26,34].

Shock velocity (U_s) versus particle velocity (U_p) from this work and Refs. [12–16] is plotted in Fig. 2(a). Carbon dioxide is predicted to have at least three phases in the shocked fluid regime [17]. The low-pressure [$U_s < 10$ km/s, blown up in Fig. 2(c)] shock wave data [12–15] cover three phases. The lowest-pressure datum [14] at 5 GPa is likely

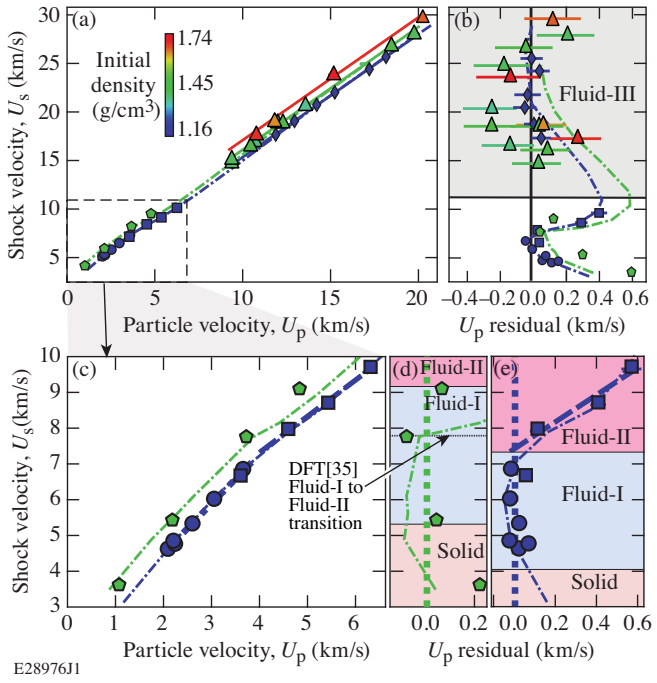

FIG. 2. (a) Shock velocity versus particle velocity. Initial density for all data and fits is given by the color bar. Triangles are these OMEGA data; diamonds are Sandia Z data [16]. Solid lines are the fit to the OMEGA and Z data. Dotted-dashed lines are density functional theory (DFT) [35]. Additionally plotted are lower-pressure shock data (circles [12]; squares [13]; pentagons [14]). (b) Residual of data and DFT to the fit to the OMEGA and Z data. (c) Blowup of the low-pressure region. Dotted green and blue lines are linear fits to the fluid-I data with a single slope. The dashed blue line is a linear fit to fluid-II data. Coefficients and covariance matrix elements for these fits are given in the Supplemental Material [33]. (d) Residual of the data from Ref. [14] and the fit to the fluid-I data for $\rho_0 = 1.45$ g/cm^3. (e) Residual of the data from Refs. [12,13] and the fit to the Fluid-I data for $\rho_0 = 1.17$ g/cm^3. Phases are described in the text.

solid; this is supported by calculated Hugoniots [35] and the measured melt line of CO_2 [9]. The $\rho_0 = 1.17$ g/cm^3 data (blue) [12,13] below $U_s = 7$ km/s and the $\rho_0 = 1.45$ g/cm^3 data (green) [14,15] below 10 km/s exhibit the same linear $U_s - U_p$ slope (dotted blue and dotted green), which suggests that they are in the same phase, denoted as fluid I. The residuals of the low-pressure data to the fluid-I fit are plotted in Figs. 2(d) ($\rho_0 = 1.45$ g/cm^3) and 2(e) ($\rho_0 = 1.17$ g/cm^3). The 1.17 g/cm^3 data undergo a clear decrease in slope above $U_s = 7$ km/s [13], as shown in the residual plot in Fig. 2(e) (dashed blue). This trend was a benchmark for density functional theory (DFT) [35] and may be attributed to a change from a molecular fluid to an insulating polymeric fluid [17]. We denote this regime as fluid II. Conversely, no such change in slope is observed in the 1.45 g/cm^3 data, indicating the threshold for the transition must be above 9.65 km/s for this initial density.

The high-pressure ($U_s > 15$ km/s) shock wave data exhibit yet another $U_s - U_p$ slope, implying that another transition(s) occurs below 15 km/s (189 GPa). That transition must produce both a shift and change in slope (or multiple slope changes) as predicted by DFT [35] (dotted-dashed lines), suggesting complex behavior relating to high-pressure chemistry. We performed a linear fit to all existing data between 189 and 995 GPa (our OMEGA data and data from Ref. [16]), including a linear term to account for the initial density (ρ_0) of each point:

$$U_s(U_p, \rho_0) = c_0 + sU_p + a\rho_0 \quad (1)$$

Coefficients and covariance matrix elements for this fit are presented in the Supplemental Material [33]. The high-pressure ($U_s > 15$ km/s) data fall within two standard deviations of the fit, or a residual 0.32 km/s as shown in Fig. 2(b). We denote this regime as fluid III. We cannot rule out that other transitions may exist between $U_s = 9.65$ and 14.72 km/s, since there are currently no data to constrain this region.

The impedance matching results are shown in pressure-versus-compression (ρ/ρ_0) space in Fig. 3. As initial density increases, the CO_2 Hugoniot becomes stiffer. DFT calculations (dotted-dashed lines) [35] agree well with the $\rho_0 = 1.17$ g/cm^3 data (blue), but the higher-initial-density CO_2 data (green) exhibit less compressibility than that model [35] predicts between 50 and 500 GPa. More-recent LEOS (Livermore equation of state) fits [36] (dashed) match the OMEGA $\rho_0 = 1.4$ and 1.7 g/cm^3 data (green and red triangles), but they do not predict the increase in compressibility seen by Nellis *et al.* [13] (blue squares) above 30 GPa.

The self-emission (590 to 850 nm) from the shock was measured using streaked optical pyrometry (SOP) [37]. The brightness temperature was determined from the self-emission and reflectance of the CO_2 shocks, which were

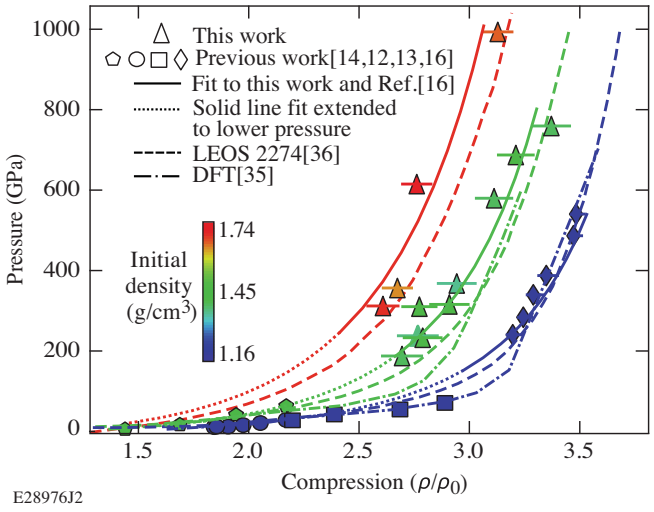

FIG. 3. Pressure versus compression (ρ/ρ_0) for shocked CO_2. Triangles are these OMEGA data; diamonds are Sandia Z data [16]. Additionally plotted are lower-pressure shock data (circles [12], squares [13], pentagons [14]). Solid lines are our linear $U_s(U_p, \rho_0)$ fit given by Eq. (1); dotted lines extend this fit below 189 GPa, the lowest-pressure data point of the fit. Dotted-dashed lines are DFT calculations [35], and dashed lines are LEOS models [36]. Initial density for all data and fits is given by the color bar.

referenced to those in quartz [28,38]. Figure 4(a) shows the average temperature for initially 1.4 g/cm^3 CO_2 (solid green) and 1.7 g/cm^3 CO_2 (solid red); the uncertainty in both temperature and reflectivity was defined as the standard deviation in individual shock velocity bins (75 total bins). Data and total uncertainty for the temperature and reflectivity of individual shots is presented in the Supplemental Material [33].

The shock reflectivity at 532 nm, deduced from the VISAR amplitude and intensity as referenced to the known reflectivity of the quartz standard [28,38], is inset in Fig. 4(a). The reflectivity rises steeply from a few percent at 100 GPa to saturation at 32% above 200 GPa, lower than the theory-predicted saturation of 40% [35] (open black circles). The steep rise is a result of the insulator-to-conductor transition driven by increasing pressure and temperature. Previous theoretical work predicted the onset of metallization to occur as low as 20 GPa [40]. We propose that metallization begins in fluid III, above 100 GPa on the Hugoniot. A multiphase fluid regime is constructed in Fig. 4(a) based on trends in the shock velocity of CO_2 in conjunction with theoretical calculations from Ref. [17] that predict a four-fluid system. The predicted boundaries of these fluids were adjusted to be consistent with the observed data.

We infer the dc electrical conductivity plotted in Fig. 4(b) from a Smith-Drude model. This modification to the Drude free-electron model employs a backscattering parameter c to capture non-Drude-like reductions in

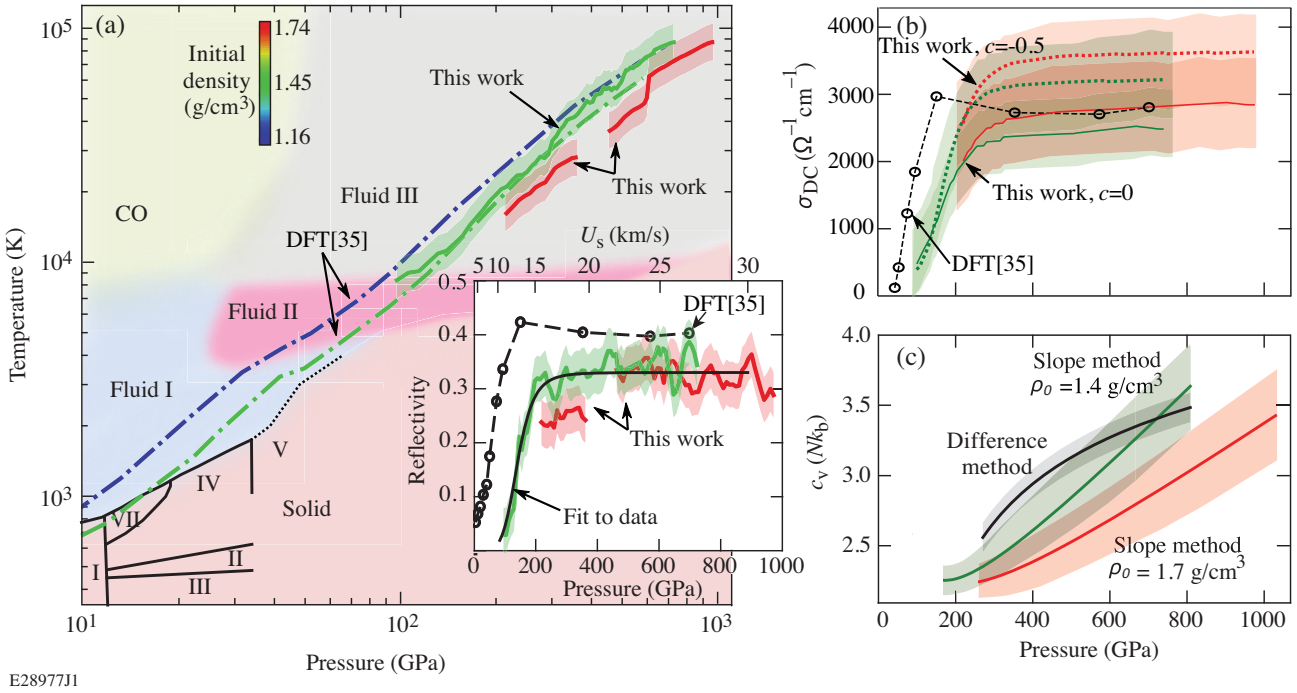

FIG. 4. (a) Red and green solid lines are average decaying-shock temperature versus pressure for the present study, with shading representing random uncertainty and the color specifying initial density (color bar). Dotted-dashed lines are from theory [35]. Solid black lines are measured phase boundaries [7,9], and the dotted black line is a calculated continuation of the melt curve [39]. Shaded regions indicate phases as described in the text. Inset: average reflectivity at 532 nm versus pressure for the decaying shocks. The shock velocity axis (top) is mapped from the pressure axis (bottom) using Eq. (1) for $\rho_0 = 1.4$ g/cm^3 and the Rankine-Hugoniot conditions. The solid black line is a Hill fit to all of the reflectivity versus shock velocity data. DFT (open circles connected by a dashed line) [35] predicts a lower-pressure threshold for the insulating-to-conducting transition and higher reflectivity upon saturation. (b) The dc conductivity for these data is inferred from our measured reflectivites by a Smith-Drude model with $c = 0$ (solid) and $c = -0.5$ (dotted). Additionally plotted is the DFT-predicted conductivity of CO_2 (black open circles) [35]. (c) Green (red) is isochoric specific heat (c_v) determined from the slope of the Hugoniot with initial density 1.4 (1.7) g/cm^3, and black is c_v as determined from a difference method between the two Hugoniots. Shading represents a 1σ confidence interval.

electron velocity [41,42]. The electron density is defined as $n_e = zn_i$, and the ionization z is varied until the model yields the measured reflectivity. Utilizing the Fresnel reflectivity and a minimum scattering time from the Ioffe Regel limit [43–45], the dc conductivity saturates to 2500 Ω^{-1} cm^{-1} and the inferred carrier density tends toward 0.3 e^-/atom of atomic CO_2 for minimum backscattering ($c = 0$). Ionization tends to unity and dc conductivity saturates to 3500 Ω^{-1} cm^{-1} for moderate backscattering of $c = -0.5$. We assume the scattering to be from fully dissociated CO_2 in the model; if molecular CO_2 was the cause of the scattering, the dc conductivity would decrease by approximately 250 Ω^{-1} cm^{-1}. We predict that at a higher temperature, the reflectivity and conductivity would experience another rise as we reach a regime in which additional charge carriers contribute to the conductivity. This behavior will lead to some eventual saturation until the carriers are no longer degenerate.

The range of initial densities provides Hugoniots for both initially solid and liquid CO_2 and facilitates calculations of thermodynamic derivatives using both a slope method and a difference method at a constant volume [38]. From the mechanical equation of state given by Eq. (1), we calculated the average CO_2 Gruneisen parameter over the pressure range studied to be $\gamma = V(\partial P/\partial E)|_V = 0.63 \pm 0.04$. This value is close to that found both experimentally and theoretically for SiO_2 at 1 TPa and 60 000 K [26,38].

Simultaneous temperature measurements allow one to calculate the isochoric specific heat $c_v = (\partial E/\partial T)|_V$. The slope method [38] allows for the calculation of the specific heat along the Hugoniot of initially liquid (green, $\rho_0 = 1.4$ g/cm^3) and initially solid (red, $\rho_0 = 1.7$ g/cm^3) CO_2. As plotted in Fig. 4(c), the specific heat is steadily increasing from 200 GPa to 1 TPa for both initially liquid and solid CO_2. The difference method (black), independent from the slope method, corroborates the trend of increasing specific heat. Uncertainties in thermodynamic derivatives were propagated from the uncertainties in pressure, density, internal energy, and temperature using a 100 000 trial Monte Carlo method. Increasing specific heat indicates increasing degrees of freedom with increasing temperature in the fluid; because reflectivity is constant above 200 GPa, the increasing degrees of freedom is not due to a rapidly

rising carrier density. We conclude that the electrically conducting fluid-III phase consists of a moderately ionized and bonded species of increasing chemical complexity, rather than a simple atomic fluid undergoing increasing ionization.

In summary, the present work extends pressure and density measurements of the initially liquid and initially solid CO_2 Hugoniot to 1 TPa and provides the first temperature measurements of shocked CO_2 to 93 000 K. We propose a fluid phase diagram comprising at least three regimes to describe existing shocked CO_2 data. Reflectivity and specific heat trends indicate that at pressures reaching 1 TPa, CO_2 is not likely a simple atomic fluid but instead a complex bonded and partially ionized species. Current models do not predict the observed compressibility and metallization behavior of high-pressure CO_2. The present work demonstrates the rich behavior of nominally simple materials at high energy density, and invites further inquiry into the chemistry of warm dense matter.

This material is based upon work supported by the Department of Energy National Nuclear Security Administration under Award No. DE-NA0003856, the University of Rochester, the New York State Energy Research and Development Authority, and NNSA support to the University of California, Berkeley. Target fabrication was conducted at LLNL HED Science Center Technology Facility. This work was performed under the auspices of the U.S. Department of Energy by Lawrence Livermore National Laboratory under Contract No. DE-AC52-07NA27344 and was supported by the LLNL-LDRD Program under Project No. 12-SI-007. The authors thank P. Loubeyre for his significant contribution in developing the experimental platform used in this work. This report was prepared as an account of work sponsored by an agency of the U.S. Government. Neither the U.S. Government nor any agency thereof, nor any of their employees, makes any warranty, express or implied, or assumes any legal liability or responsibility for the accuracy, completeness, or usefulness of any information, apparatus, product, or process disclosed, or represents that its use would not infringe privately owned rights. Reference herein to any specific commercial product, process, or service by trade name, trademark, manufacturer, or otherwise does not necessarily constitute or imply its endorsement, recommendation, or favoring by the U.S. Government or any agency thereof. The views and opinions of authors expressed herein do not necessarily state or reflect those of the U.S. Government or any agency thereof.

[1] T. Guillot, Science **286**, 72 (1999).
[2] C. Cavazzoni, G. L. Chiarotti, S. Scandolo, E. Tosatti, M. Bernasconi, and M. Parrinello, Science **283**, 44 (1999).
[3] S. Stanley and J. Bloxham, Nature (London) **428**, 151 (2004).
[4] M. van Thiel and F. H. Ree, J. Appl. Phys. **62**, 1761 (1987).
[5] V. V. Chaban, E. E. Fileti, and O. V. Prezhdo, J. Phys. Chem. Lett. **6**, 913 (2015).
[6] K. F. Dziubek, M. Ende, D. Scelta, R. Bini, M. Mezouar, G. Garbarino, and R. Miletich, Nat. Commun. **9**, 3148 (2018).
[7] F. Datchi and G. Weck, Z. Kristallogr. **229**, 135 (2014).
[8] C.-S. Yoo, Phys. Chem. Chem. Phys. **15**, 7949 (2013).
[9] K. D. Litasov, A. F. Goncharov, and R. J. Hemley, Earth Planet. Sci. Lett. **309**, 318 (2011).
[10] V. M. Giordano, F. Datchi, F. A. Gorelli, and R. Bini, J. Chem. Phys. **133**, 144501 (2010).
[11] V. M. Giordano, F. Datchi, and A. Dewaele, J. Chem. Phys. **125**, 054504 (2006).
[12] G. L. Schott, High Press. Res. **6**, 187 (1991).
[13] W. J. Nellis, A. C. Mitchell, F. H. Ree, M. Ross, N. C. Holmes, R. J. Trainor, and D. J. Erskine, J. Chem. Phys. **95**, 5268 (1991).
[14] V. N. Zubarev and G. S. Telegin, Sov. Phys.-Dokl. **7**, 34 (1962).
[15] Zubarev and Telegin [14] report two different initial densities for their solid CO_2: 1.45 and 1.54 g/cm^3. Cited in Schott [12] are "verbal inquires and replies conveyed through C. L. Mader and A. N. Dremin, ca. 1983" that confirm that 1.54 g/cm^3 is a misprint, and the initial density of the data published by Zubarev and Telegin is 1.45 g/cm^3.
[16] S. Root, K. R. Cochrane, J. H. Carpenter, and T. R. Mattsson, Phys. Rev. B **87**, 224102 (2013).
[17] B. Boates, A. M. Teweldeberhan, and S. A. Bonev, Proc. Natl. Acad. Sci. U.S.A. **109**, 14808 (2012).
[18] T. R. Boehly, D. L. Brown, R. S. Craxton, R. L. Keck, J. P. Knauer, J. H. Kelly, T. J. Kessler, S. A. Kumpan, S. J. Loucks, S. A. Letzring *et al.*, Opt. Commun. **133**, 495 (1997).
[19] G. J. Piermarini, S. Block, J. D. Barnett, and R. A. Forman, J. Appl. Phys. **46**, 2774 (1975).
[20] P. Loubeyre, P. M. Celliers, D. G. Hicks, E. Henry, A. Dewaele, J. Pasley, J. Eggert, M. Koenig, F. Occelli, K. M. Lee *et al.*, High Press. Res. **24**, 25 (2003).
[21] J. Eggert, S. Brygoo, P. Loubeyre, R. S. McWilliams, P. M. Celliers, D. G. Hicks, T. R. Boehly, R. Jeanloz, and G. W. Collins, Phys. Rev. Lett. **100**, 124503 (2008).
[22] P. M. Celliers, P. Loubeyre, J. H. Eggert, S. Brygoo, R. S. McWilliams, D. G. Hicks, T. R. Boehly, R. Jeanloz, and G. W. Collins, Phys. Rev. Lett. **104**, 184503 (2010).
[23] P. Loubeyre, S. Brygoo, J. Eggert, P. M. Celliers, D. K. Spaulding, J. R. Rygg, T. R. Boehly, G. W. Collins, and R. Jeanloz, Phys. Rev. B **86**, 144115 (2012).
[24] S. M. Sterner and K. S. Pitzer, Contrib. Mineral. Petrol. **117**, 362 (1994).
[25] P. M. Celliers, D. K. Bradley, G. W. Collins, D. G. Hicks, T. R. Boehly, and W. J. Armstrong, Rev. Sci. Instrum. **75**, 4916 (2004).
[26] M. D. Knudson and M. P. Desjarlais, Phys. Rev. B **88**, 184107 (2013).
[27] M. P. Desjarlais, M. D. Knudson, and K. R. Cochrane, J. Appl. Phys. **122**, 035903 (2017).
[28] S. Brygoo, M. Millot, P. Loubeyre, A. E. Lazicki, S. Hamel, T. Qi, P. M. Celliers, F. Coppari, J. H. Eggert, D. E. Fratanduono *et al.*, J. Appl. Phys. **118**, 195901 (2015).

[29] Ya. B. Zeldovich and Yu. P. Razer, in *Physics of Shock Waves and High-Temperature Hydrodynamic Phenomena*, edited by W. D. Hayes and R. F. Probstein (Dover Publications, Mineola, NY, 2002).
[30] C. A. McCoy, M. C. Gregor, D. N. Polsin, D. E. Fratanduono, P. M. Celliers, T. R. Boehly, and D. D. Meyerhofer, J. Appl. Phys. **119**, 215901 (2016).
[31] C. Meade and R. Jeanloz, Phys. Rev. B **35**, 236 (1987).
[32] R. G. Kraus, S. T. Stewart, D. C. Swift, C. A. Bolme, R. F. Smith, S. Hamel, B. D. Hammel, D. K. Spaulding, D. G. Hicks, J. H. Eggert *et al.*, J. Geophys. Res. **117**, E09009 (2012).
[33] See the Supplemental Material at http://link.aps.org/supplemental/10.1103/PhysRevLett.125.165701 for the fused silica isentropic release.
[34] C. A. McCoy, M. C. Marshall, D. N. Polsin, D. E. Fratanduono, P. M. Celliers, D. D. Meyerhofer, and T. R. Boehly, Phys. Rev. B **100**, 014106 (2019).
[35] B. Boates, S. Hamel, E. Schwegler, and S. A. Bonev, J. Chem. Phys. **134**, 064504 (2011).
[36] C. J. Wu, D. A. Young, P. A. Sterne, and P. C. Myint, J. Chem. Phys. **151**, 224505 (2019).
[37] J. E. Miller, T. R. Boehly, A. Melchior, D. D. Meyerhofer, P. M. Celliers, J. H. Eggert, D. G. Hicks, C. M. Sorce, J. A. Oertel, and P. M. Emmel, Rev. Sci. Instrum. **78**, 034903 (2007).
[38] D. G. Hicks, T. R. Boehly, J. H. Eggert, J. E. Miller, P. M. Celliers, and G. W. Collins, Phys. Rev. Lett. **97**, 025502 (2006).
[39] A. M. Teweldeberhan, B. Boates, and S. A. Bonev, Earth Planet Sci. Lett. **373**, 228 (2013).
[40] C. Wang and P. Zhang, J. Chem. Phys. **133**, 134503 (2010).
[41] N. V. Smith, Phys. Rev. B **64**, 155106 (2001).
[42] R. S. McWilliams, D. A. Dalton, M. F. Mahmood, and A. F. Goncharov, Phys. Rev. Lett. **116**, 255501 (2016).
[43] P. M. Celliers, G. W. Collins, D. G. Hicks, M. Koenig, E. Henry, A. Benuzzi-Mounaix, D. Batani, D. K. Bradley, L. B. Da Silva, R. J. Wallace *et al.*, Phys. Plasmas **11**, L41 (2004).
[44] D. G. Hicks, P. M. Celliers, G. W. Collins, J. H. Eggert, and S. J. Moon, Phys. Rev. Lett. **91**, 035502 (2003).
[45] M. Millot, S. Hamel, J. R. Rygg, P. M. Celliers, G. W. Collins, F. Coppari, D. E. Fratanduono, R. Jeanloz, D. C. Swift, and J. H. Eggert, Nat. Phys. **14**, 297 (2018).